Nonlinear Dyn
https://doi.org/10.1007/s11071-018-4116-2

ORIGINAL PAPER

Nonlinear dynamic characteristics of a micro-vibration fluid viscous damper

Xiaolei Jiao · Yang Zhao · Wenlai Ma

Received: 8 July 2017 / Accepted: 27 January 2018

Abstract This study is concerned with the nonlinear dynamic characteristics of a micro-vibration fluid viscous damper used in a satellite. When a control moment gyroscope is working, it produces micro-vibrations, which is a disadvantage for imaging equipment. Taking a single-tube micro-vibration fluid viscous damper as our research subject, a nonlinear dynamic model of the micro-vibration fluid viscous damper under harmonic excitation is proposed. Then, the analytical form of the pressure gradient force is derived. Considering the entrance effect in the orifice, the nonlinear elastic force and nonlinear damping force are analyzed. The results reveal that if the entrance effect is not considered, the elastic force and damping force are linear forces. When the entrance effect is considered, the damper has a nonlinear elastic force and a nonlinear damping force. These nonlinear forces are related to the orifice length, diameter, fluid viscosity, excitation amplitude and frequency. In the low-frequency domain, the differences between the two cases are small, while in the high-frequency domain, they are considerable.

X. Jiao (✉) · Y. Zhao · W. Ma
School of Astronautics, Harbin Institute of Technology, Harbin 150001, China
e-mail: jiaoxiaoleib@163.com

Y. Zhao
e-mail: yangzhao@hit.edu.cn

W. Ma
e-mail: mawenlai2000@sina.com

Keywords Micro-vibration · Fluid viscous damper · Nonlinear damping force · Nonlinear elastic force

1 Introduction

When the control moment gyroscope (CMG) of a satellite is working, it produces high-frequency micro-vibrations that have a serious effect on imaging equipment. It is necessary to prevent micro-vibrations produced by the CMG. The typical methods for isolating micro-vibrations are passive isolation, active isolation, and hybrid isolation. Passive isolation is used widely. Commonly used passive dampers include viscoelastic material dampers [1] and fluid viscous dampers [2,3]. Active dampers include electromagnetic dampers [4–6], and hybrid dampers include voice coil dampers [7,8]. Although active dampers and hybrid dampers perform well, they are not reliable. In addition, they need additional energy equipment and control strategies. Therefore, active dampers and hybrid dampers are not widely used in micro-vibration isolation. In contrast, passive dampers have perfect reliability and are simple structures, so they are widely used. The performance of a viscoelastic material damper is sensitive to the temperature, and the damper requires a high-performance temperature control system in a satellite. Therefore, a fluid viscous damper is a reasonable choice.

A fluid viscous damper usually produces damping forces using a damping orifice or annular clearance.

Published online: 06 February 2018

When fluid passes through the orifice or annular clearance, the damper produces a pressure gradient force. If the length of the orifice or annular clearance is long, it is unnecessary to consider the entrance effect of the orifice, but when the length of the orifice is short, it is necessary to consider the entrance effect.

Because the structure of fluid viscous damper is simple, it is used widely in micro-vibration isolation. It was first used in the aerospace industry to isolate micro-vibrations in the Hubble telescope. This micro-vibration fluid viscous damper is called a D-strut and is produced by the Honeywell company [2,3]. When silicon oil passes through the orifice, there are different pressures in the two cavities. A damping force is produced because of the pressure gradient between the two cavities. Two bellows are used to provide the main stiffness. Due to the perfect viscosity–temperature characteristics of silicon oil, the D-strut has perfect performance. In recent years, there have been many studies on micro-vibration fluid viscous dampers used in satellites. Wang [9] studied the micro-vibration fluid viscous damper based on a three-parameter system, in which the harmonic balance method was used to solve nonlinear equations. Shi [10] studied a fluid viscous damper that had a bellows structure. A dynamic model of this damper was established, in which nonlinear stiffness and damping were equivalent to linear stiffness and damping. Narkhede [11] studied the shock dynamic characteristics of a nonlinear fluid viscous damper that had an annular clearance, but the study focused on non-Newtonian fluids. Hou [12] studied the nonlinear dynamic characteristics of a fluid viscous damper that had an annular clearance. Hou thought that the nonlinear damping and stiffness were the result of shear thinning. Zhang [13] proposed the concept of the output frequency response function (OFRF) based on studying a cubic fluid viscous damper. The results indicated that a damper that contained cubic damping had perfect performance in isolating vibrations produced by structures with multiple degrees of freedom. Wolfe [14] studied parameter identification in a large-scale nonlinear fluid viscous damper. Farjoud [15] proposed a nonlinear dynamic model of a single-tube fluid viscous damper. Hou [16] proposed a nonlinear dynamic model of an annular clearance damper based on the Navier–Stokes equations, and Hou analyzed the effects of viscosity and frequency on the damper response. Narkhede [17] studied the dynamic characteristics of nonlinear dampers under impulse excitation. Shum [18] studied the nonlinear viscous damper under random excitation and proposed a design method for this damper. Guo [19] analyzed the force and displacement transmissibility of a nonlinear viscous damper. The transmissibility was derived using the Ritz–Galerkin method, but this model is based on a lumped-parameter system. Lang [20] studied a fluid viscous damper that contained cubic damping using the OFRF and a lumped-parameter system. Lv [21] studied a single degree of freedom (SDOF) nonlinear fluid viscous damper vibration system and analyzed the steady-state response.

In short, previous studies of nonlinear viscous dampers have focused on lumped-parameter systems. Nonlinear dynamic equations have been solved with the harmonic balance method or other methods. There are not enough studies on the mechanisms of nonlinear damping and nonlinear stiffness.

This paper focuses on analyzing the mechanism of the nonlinear damping and nonlinear elastic forces of a micro-vibration fluid viscous damper. The objective is to extend the study of the mechanism of nonlinear damping and nonlinear stiffness. To achieve this goal, a single-tube damper is used as our research subject, and a nonlinear dynamic model of a micro-vibration fluid viscous damper that considers the entrance effect is proposed. Then, an inverse Laplace transform is applied to obtain the nonlinear damping force and nonlinear elastic force. The results reveal that when the entrance effect is considered, the damper has a nonlinear elastic force and nonlinear damping force. These forces are related to the orifice length, diameter, fluid viscosity, excitation amplitude, and frequency.

2 Dynamic model of the single-tube micro-vibration fluid viscous damper

When a fluid passes through an orifice, the fluid in the orifice is laminar ($Re < Re_{\mathrm{cr}}$, where Re_{cr} is the critical Reynolds number). Because of the wall boundary condition at the wall, the velocity near the wall is zero, while the fluid in the middle of the pipe has the largest velocity. Considering a micro-fluid column in the pipe and analyzing the forces that act on this micro-column, the resistance of the pipe can be obtained.

$$R_h = \frac{128\mu l}{\pi d^4} \tag{1}$$

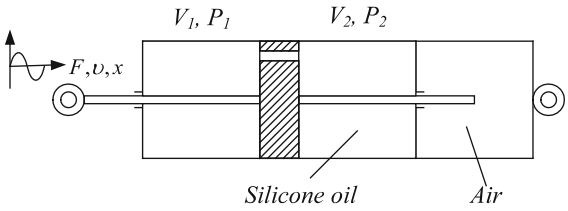

Fig. 1 Model of a single-tube fluid viscous damper

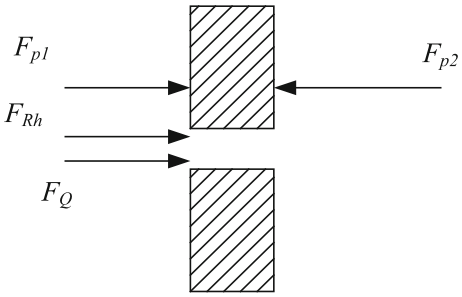

Fig. 2 Forces on the piston

where μ represents the viscosity, l represents the length, and d represents the diameter. A single-tube fluid viscous damper [22] is illustrated in Fig. 1. The piston in the middle of tube divides the cavity into two parts, the left part and the right part. When a sinusoidal excitation acts on the piston, it squeezes the silicone oil in the damper, which produces a pressure gradient force because of the different pressures in the two cavities. V_1 is the volume of the left cavity, and V_2 is the volume of the right cavity. P_1 and P_2 are the pressures of the two cavities. F_{P1} and F_{P2} are the forces of the two cavities. F_{Rh} is the force produced by the resistance in the orifice, as shown in Fig. 2. F_Q is the inertia force of the fluid column in the orifice.

When silicone oil flows in the cavity, a part of the fluid passes through the orifice from one cavity to another cavity, while the rest of the fluid is compressed.

According to flux conservation

$$\begin{cases} -Q + A_{\mathrm{P}}\upsilon = \frac{1}{\beta} V_1 \dot{P}_1 \\ Q - A_{\mathrm{P}}\upsilon = \frac{1}{\beta} V_2 \dot{P}_2 \end{cases} \tag{2}$$

In this equation, Q is the flow rate in the orifice, A_{P} is the area of the piston, υ is the velocity of the piston, and β is the bulk modulus of the silicon oil.

Because the viscosity of the silicon oil in the damper is large and the flow in the orifice is laminar, the force equilibrium equation of the liquid column in the orifice can be written as

$$\begin{cases} \rho L_g \dot{Q} + R_h Q A_g = (P_1 - P_2) A_g \\ R_h = 128 \frac{\mu L_g}{\pi d^4} \end{cases} \tag{3}$$

where ρ is the density of the silicon oil, L_g is the length of the orifice, A_g is the area of the orifice, and R_h is the resistance.

If the excitation is the velocity, it can be described as

$$\upsilon = \upsilon_0 \sin(\omega t) \tag{4}$$

where υ_0 is the amplitude of the velocity, and ω is the circular frequency. F is the pressure gradient force and can be written as

$$F = (P_1 - P_2) A_P \tag{5}$$

The state equation of the system can be described as

$$\dot{X} = AX + B\upsilon$$
$$A = \begin{bmatrix} 0 & 0 & -\frac{\beta}{V_1} \\ 0 & 0 & \frac{\beta}{V_2} \\ \frac{A_g}{\rho L_g} & -\frac{A_g}{\rho L_g} & 0 \end{bmatrix}, B = \begin{bmatrix} 0 & 0 & \beta \frac{A_P}{V_1} \\ 0 & 0 & -\beta \frac{A_P}{V_1} \\ 0 & 0 & 0 \end{bmatrix} \tag{6}$$

For micro-vibrations, the amplitude of the displacement is small, and therefore the volumes of two cavities are constant: $V_1 = V_2 = V_0$.

$$\Omega_{\mathrm{F}} = \sqrt{2 \frac{\beta}{V_0} \frac{A_g}{\rho L_g}} \tag{7}$$

Ω_{F} is the circular frequency of the liquid column in the orifice. It can be further written as

$$\Omega_{\mathrm{F}} = A_g \sqrt{\frac{2\beta}{V_0 m_g}} \tag{8}$$

where m_g is the mass of the liquid column in the orifice. The transfer function can be written as

$$\Phi(s) = \frac{F(\mathrm{s})}{\upsilon(s)} = \frac{\frac{2\beta A_P^2}{V_0}\left(s + \frac{R_h A_g}{\rho L_g}\right)}{s^2 + R_h \frac{A_g}{\rho L_g} s + 2 \frac{A_g}{\rho L_g} \frac{\beta}{V_0}} \tag{9}$$
$$\upsilon = \dot{x}, \upsilon(s) = sX(s)$$

Because $\upsilon(s) = sX(s)$, Eq. (9) can be written as

$$\Phi(s) = \frac{F(\mathrm{s})}{sX(s)} = \frac{2\beta A_P^2}{V_0} \frac{\left(s + \frac{R_h A_g}{\rho L_g}\right)}{s^2 + R_h \frac{A_g}{\rho L_g} s + 2 \frac{A_g}{\rho L_g} \frac{\beta}{V_0}} \tag{10}$$

It can be further written as

$$\frac{F\,(\mathrm{s})}{X\,(s)} = \frac{2\beta A_P^2}{V_0} \frac{s\left(s + \frac{R_h A_g}{\rho L_g}\right)}{s^2 + R_h \frac{A_g}{\rho L_g} s + 2\frac{A_g}{\rho L_g}\frac{\beta}{V_0}} \tag{11}$$

It can be seen from denominator of Eq. (11) that the characteristic root has a relationship with R_h, A_g, L_g, ρ, β, V. If these parameters take different values, the pressure gradient force will be different. Therefore, it is necessary to analyze the distribution of the characteristic roots.

$$\Delta = A_2^2 - 4A_3 = \left(\frac{R_h A_g}{\rho L_g}\right)^2 - \frac{8\beta A_g}{\left(\rho L_g\right) V_0}$$
$$A_1 = \frac{R_h A_g}{\rho L_g}, A_2 = \frac{R_h A_g}{\rho L_g}, A_3 = \frac{2\beta A_g}{\rho L_g V_0} \tag{12}$$

Equation (12) is a discriminant.

(1) If $\Delta < 0$, the transfer function has a pair of conjugate complex roots. The conjugate complex roots can be described as

$$s_1 = a + bj, s_2 = a - bj$$
$$a = -\frac{A_2}{2}, b = \frac{\sqrt{A_2^2 - 4A_3}}{2}$$

Equation (11) can be rewritten as:

$$\frac{F\,(\mathrm{s})}{X\,(s)} = K_0 \frac{s^2 + A_1 s}{(s - s_1)\,(s - s_2)} \tag{13}$$

Using an inverse Laplace transform, the pressure gradient force can be obtained.

$$F\,(t) = K_0 x_0 \omega \left[\begin{array}{l} 2U\cos(\omega t) - 2V\sin(\omega t) \\ +2e^{at}\left(\begin{array}{l} M_s\cos(bt) - \\ N_s\sin(bt) \end{array}\right) \end{array}\right]$$
$$K_0 = \frac{2\beta A_p^2}{V_0}, A_1 = \frac{R_h A_g}{\rho L_g}, A_2 = \frac{R_h A_g}{\rho L_g}$$
$$A_3 = \frac{2\beta A_g}{\rho L_g V_0}, B_1 = -\omega^2, B_2 = A_1\omega$$
$$B_3 = 4a\omega^2, B_4 = 2\omega\left(a^2 - \omega^2 + b^2\right)$$
$$N_1 = a^2 - b^2 + A_1 a, N_2 = 2ab + A_1 b$$
$$N_3 = -4ab^2, N_4 = 2b\left(a^2 - \omega^2 + b^2\right)$$
$$U = \frac{B_1 B_3 + B_2 B_4}{B_3^2 + B_4^2}, V = \frac{B_2 B_3 - B_1 B_4}{B_3^2 + B_4^2}$$
$$M_s = \frac{N_1 N_3 + N_2 N_4}{N_3^2 + N_4^2}, N_s = \frac{N_2 N_3 - N_1 N_4}{N_3^2 + N_4^2} \tag{14}$$

(2) If $\Delta > 0$, there are two different real roots, which can be written as

$$s_1 = -\frac{A_2}{2} + \frac{\sqrt{A_2^2 - 4A_3}}{2}$$
$$s_2 = -\frac{A_2}{2} - \frac{\sqrt{A_2^2 - 4A_3}}{2}$$

The transfer function can be written as

$$\frac{F\,(\mathrm{s})}{X\,(s)} = K_0 \frac{s^2 + A_1 s}{(s - s_1)\,(s - s_2)} \tag{15}$$

Using an inverse Laplace transform, the time response of the pressure gradient force can be obtained.

$$F\,(t) = K_0 x_0 \omega \left[\begin{array}{l} 2U\cos(\omega t) - 2V\sin(\omega t) + \\ c_3 e^{s_1 t} + c_4 e^{s_2 t} \end{array}\right]$$
$$K_0 = \frac{2\beta A_p^2}{V_0}, B_1 = -\omega^2, B_2 = A_1\omega$$
$$B_3 = 2\omega^2\left(s_1 + s_2\right), B_4 = 2\omega\left(s_1 s_2 - \omega^2\right)$$
$$U = \frac{B_1 B_3 + B_2 B_4}{B_3^2 + B_4^2}, V = \frac{B_2 B_3 - B_1 B_4}{B_3^2 + B_4^2}$$
$$c_3 = \frac{s_1^2 + A_1 s_1}{\left(s_1^2 + \omega^2\right)(s_1 - s_2)}, c_4 = \frac{s_2^2 + A_1 s_2}{\left(s_1^2 + \omega^2\right)(s_1 - s_2)} \tag{16}$$

(3) If $\Delta = 0$, the two real roots are the same. They can be written as

$$s_1 = s_2 = -\frac{A_2}{2}, n = -\frac{A_2}{2}$$

The transfer function can be written as

$$\frac{F\,(\mathrm{s})}{X\,(s)} = K_0 \frac{s^2 + A_1 s}{(s - s_1)\,(s - s_2)} \tag{17}$$

Using an inverse Laplace transform, the pressure gradient force can be obtained.

$$F\,(t) = K_0 x_0 \omega \left[\begin{array}{l} 2U\cos(\omega t) - 2V\sin(\omega t) + \\ (c_3 t + c_4)\, e^{nt} \end{array}\right]$$
$$B_1 = -\omega^2, B_2 = A_1\omega, B_3 = 4n\omega^2$$
$$B_4 = 2n^2\omega - 2\omega^3, c_3 = \frac{n^2 + nA_1}{n^2 + \omega^2}$$
$$c_4 = \frac{2n^3}{\left(n^2 + \omega^2\right)^2}, U = \frac{B_1 B_3 + B_2 B_4}{B_3^2 + B_4^2},$$
$$V = \frac{B_2 B_3 - B_1 B_4}{B_3^2 + B_4^2} \tag{18}$$

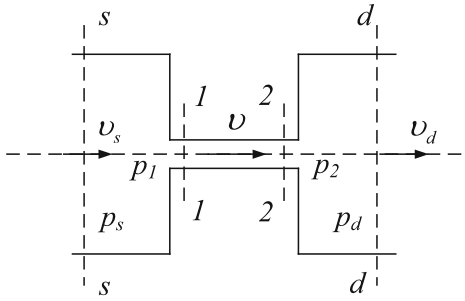

Fig. 3 Entrance effect

3 Entrance effect in the orifice

The dynamic model derived in Sect. 2 does not consider the entrance effect in the orifice. When the length of the orifice is large, this is reasonable. For a shorter orifice, it is necessary to consider the entrance effect in the orifice. In this section, a dynamic model that considers the entrance effect in the orifice will be derived.

When the fluid flows from a large cavity into a short damping orifice, the energy loss near the entrance is different from the energy loss in the fully extended segment. Near the entrance of the damping orifice, energy losses include viscosity loss and kinetic energy loss. Because the length of this segment is long for laminar flow, it is necessary to consider the entrance effect.

The model that considers the entrance effect in the orifice can be analyzed using the structure shown in Fig. 3. $s-s$ is the cross section near the entrance, and $d-d$ is the cross section near the exit. p_s, υ_s, p_d, υ_d are the pressures and velocities of the respective cross sections. 1–1 is the entrance of the orifice, and 2–2 is the exit of the orifice. p_1 and p_2 are the pressures of these two cross sections. $\upsilon$is the velocity in the orifice. According to the Bernoulli equation

$$\frac{p_s}{\rho g}+\frac{\alpha_s \upsilon_s^2}{2g}=\frac{p_1}{\rho g}+\frac{\alpha \upsilon^2}{2g}+\zeta_1\frac{\upsilon^2}{2g} \tag{19}$$

where ζ_1 is the local resistance coefficient of the entrance. The pressure loss between the cross sections $s-s$ and $d-d$ can be written as

$$\Delta p_{s-d}=p_s-p_d=\frac{128\mu L_g Q}{\pi d^4}\left[1+\xi\frac{Re}{64}\left(\frac{d}{L_g}\right)\right] \tag{20}$$

where Q is the flow rate in the orifice, L_g is the length of the orifice, μ is the viscosity of the silicone oil, $d$is the diameter of the orifice, Re is the Reynolds number, and ξ' and c are correction coefficients. The pressure loss in the orifice can be written as

$$\begin{aligned}\Delta p_{1-2}=p_1-p_2&=\frac{128\mu L_g Q}{\pi d^4}\left[1+\xi'\frac{Re}{64}\left(\frac{d}{l}\right)\right]\\&=c\frac{128\mu L_g Q}{\pi d^4}\end{aligned} \tag{21}$$

The resistance can be written as

$$R_h'=cR_h,\ c=1+\xi'\frac{Re}{64}\left(\frac{d}{L_g}\right) \tag{22}$$

According to Langhaar's experiment, the approximate value of ξ' can be written as

$$\begin{cases}\xi'=2.62\left(\frac{L_g}{\mathrm{Red}}\right)^{1/4} & \frac{L_g}{\mathrm{Red}}\le 0.058\\ \xi'=1.28 & \frac{L_g}{\mathrm{Red}}>0.058\end{cases} \tag{23}$$

The Reynolds number is

$$Re=\frac{\rho\upsilon d}{\mu}$$

Equation (23) can be written as

$$\begin{cases}\xi'=2.62\left(\frac{\mu L_g}{\rho\upsilon d^2}\right)^{1/4} & \frac{L_g}{\mathrm{Red}}\le 0.058\\ \xi'=1.28 & \frac{L_g}{\mathrm{Red}}>0.058\end{cases} \tag{24}$$

Equation (24) can be written as

$$R_h'=\begin{cases}R_h\left(1+\alpha_1\upsilon^{\frac{5}{4}}\right) & \frac{L_g}{\mathrm{Red}}\le 0.058\\ R_h\left(1+\alpha_2\upsilon\right) & \frac{L_g}{\mathrm{Red}}>0.058\end{cases} \tag{25}$$

where α_1 and α_2 are coefficients

$$\alpha_1=\frac{2.62}{64}\left(\frac{\rho d^2}{\mu L_g}\right)^{\frac{3}{4}},\ \alpha_2=\frac{1.28}{64}\frac{\rho d^2}{\mu L_g}$$

Equation (25) contains nonlinear terms. The dependence of ξ' and c on $\frac{l}{\mathrm{Red}}$ is shown in Fig. 4. When the transfer function has different characteristic roots, the response in the time domain will be different too. It is necessary to discuss the distribution of these roots. When considering the entrance effect, the resistance should be R_h'.

$$A_1=\frac{R_h' A_g}{\rho L_g},\ A_2=\frac{R_h' A_g}{\rho L_g},\ A_3=\frac{2\beta A_g}{\rho L_g V_0}$$

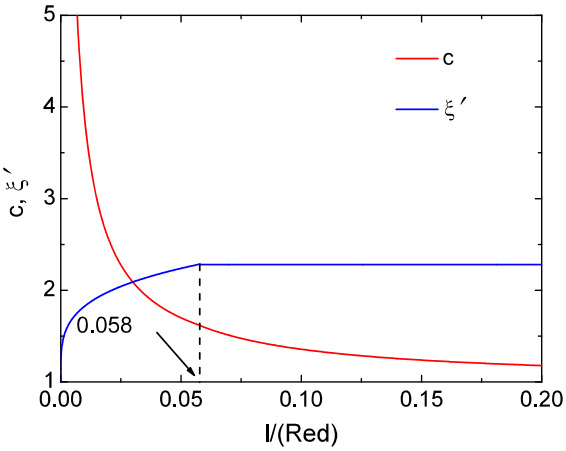

Fig. 4 Dependence of ξ' and c on $\frac{l}{\text{Red}}$

(1) When there is a pair of conjugate complex roots

$$U = \frac{A_1\left[\frac{A_1^2}{4} + \left|A_2^2 - 4A_3\right|\right]}{\left[2A_1^2\omega^2 + 2\left(\frac{A_1^2}{4} - \omega^2 + \left|A_2^2 - 4A_3\right|\right)\right]} \tag{26}$$

$$V = \frac{-K_0\omega^2\left[\left|A_2^2 - 4A_3\right| - \omega^2 - \frac{3A_1^2}{4}\right]}{A_1^2\omega^2 + \left(\frac{A_1^2}{4} - \omega^2 + \left|A_2^2 - 4A_3\right|\right)^2} \tag{27}$$

The damping force can be written as

$$F_{\text{damp}} = 2\frac{A_1\left[\frac{A_1^2}{4} + \left|A_2^2 - 4A_3\right|\right]}{\left[2A_1^2\omega^2 + 2\left(\frac{A_1^2}{4} - \omega^2 + \left|A_2^2 - 4A_3\right|\right)\right]}K_0\dot{x} \tag{28}$$

The elastic force can be written as

$$F_{\text{elastic}} = -2\frac{-K_0\omega^2\left[\left|A_2^2 - 4A_3\right| - \omega^2 - \frac{3A_1^2}{4}\right]}{A_1^2\omega^2 + \left(\frac{A_1^2}{4} - \omega^2 + \left|A_2^2 - 4A_3\right|\right)^2}K_0x$$

$$a = -\frac{A_2}{2}, b = \frac{\sqrt{A_2^2 - 4A_3}}{2} \tag{29}$$

(2) When there are two equal real roots

$$U = \frac{8A_1\omega^3 + 2A_1\left(A_1^2 - 4\omega^2\right)}{16A_1^2\omega^3 + \omega\left(A_1^2 - 4\omega^2\right)^2} \tag{30}$$

$$V = \frac{\omega\left[-\frac{3}{4}A_1^2 - \omega^2\right]}{2\left[A_1^2\omega^2 + \left(\frac{1}{4}A_1^2 - \omega^2\right)^2\right]} \tag{31}$$

The damping force can be written as

$$F_{\text{damp}} = 2\frac{8A_1\omega^3 + 2A_1\left(A_1^2 - 4\omega^2\right)}{16A_1^2\omega^3 + \omega\left(A_1^2 - 4\omega^2\right)^2}K_0\dot{x} \tag{32}$$

The elastic force can be written as

$$F_{\text{elastic}} = -2\frac{\omega\left[-\frac{3}{4}A_1^2 - \omega^2\right]}{2\left[A_1^2\omega^2 + \left(\frac{1}{4}A_1^2 - \omega^2\right)^2\right]}K_0x \tag{33}$$

(3) When there are two different real roots

$$U = \frac{2A_2\omega^4 + 2A_1\omega^2\left(-\frac{3}{4}A_2^2 + 4A_3 - \omega^2\right)}{\left(-\frac{3}{4}A_2^2 + 4A_3\right)^2 + 4\omega^2\left(-\frac{3}{4}A_2^2 + 4A_3 - \omega^2\right)^2} \tag{34}$$

$$V = \frac{-2A_1A_2\omega^3 + 2\omega^3\left(-\frac{3}{4}A_2^2 + 4A_3 - \omega^2\right)}{\left(-\frac{3}{4}A_2^2 + 4A_3\right)^2 + 4\omega^2\left(-\frac{3}{4}A_2^2 + 4A_3 - \omega^2\right)^2} \tag{35}$$

The damping force can be written as

$$F_{\text{damp}} = 2\frac{-2A_1A_2\omega^3 + 2\omega^3\left(-\frac{3}{4}A_2^2 + 4A_3 - \omega^2\right)}{\left(-\frac{3}{4}A_2^2 + 4A_3\right)^2 + 4\omega^2\left(-\frac{3}{4}A_2^2 + 4A_3 - \omega^2\right)^2}K_0\dot{x} \tag{36}$$

The elastic force can be written as

$$F_{\text{elastic}} = -2\frac{-2A_1A_2\omega^3 + 2\omega^3\left(-\frac{3}{4}A_2^2 + 4A_3 - \omega^2\right)}{\left(-\frac{3}{4}A_2^2 + 4A_3\right)^2 + 4\omega^2\left(-\frac{3}{4}A_2^2 + 4A_3 - \omega^2\right)^2}K_0x \tag{37}$$

4 Damping force, elastic force, transient force

The characteristic roots of the transfer function have a relationship with the orifice length and diameter, the size of the cavity, and the viscosity of the silicone oil. Therefore, the response in the time domain will be different. In this section, different forms of the pressure gradient force will be analyzed. Three cases are discussed. They are similar to the descriptions in Sect. 2.
(1) The transfer function has a pair of conjugate complex roots.

The pressure gradient force in the time domain can be written as

$$F(t) = F_p(t) + F_q(t) \tag{38}$$

$$F_p(t) = K_0 x_0 \omega [2U \cos(\omega t) - 2V \sin(\omega t)] \tag{39}$$

$$F_q(t) = K_0 x_0 \omega \left[2e^{at}(M_s \cos(bt) - N_s \sin(bt))\right] \tag{40}$$

$F_p(t)$ is the steady component of the pressure gradient force. $F_q(t)$ is the transient component of the pressure gradient force. The transient component decays with time. The steady component of the pressure gradient force can be written as

$$F_p(t) = F_{p\_c}(t) + F_{p\_k}(t) \tag{41}$$

where $F_{p\_c}(t)$ is the damping force and $F_{p\_k}(t)$ is the elastic force.

$$F_{p\_c}(t) = K_0 x_0 \omega [2U \cos(\omega t)] \tag{42}$$

$$F_{p\_k}(t) = -K_0 x_0 \omega [2V \sin(\omega t)] \tag{43}$$

Equations (42) and (43) can be written as

$$F_{p\_c}(t) = 2U K_0 \dot{x} \tag{44}$$

$$F_{p\_k}(t) = -2V K_0 \omega x \tag{45}$$

(2) The transfer function has two different real roots.

If the transfer function has two different real roots, the damping force, elastic force, transient force can be written as

$$F_{p\_c}(t) = K_0 x_0 \omega [2U \cos(\omega t)] \tag{46}$$

$$F_{p\_k}(t) = -K_0 x_0 \omega [2V \sin(\omega t)] \tag{47}$$

$$F_q(t) = K_0 x_0 \omega \left[(c_3 t + c_4) e^{nt}\right] \tag{48}$$

(3) The transfer function has two equal real roots.

If the transfer function has two different real roots, the damping force, elastic force and transient force can be written as

$$F_{p\_c}(t) = K_0 x_0 \omega [2U \cos(\omega t)] \tag{49}$$

$$F_{p\_k}(t) = -K_0 x_0 \omega [2V \sin(\omega t)] \tag{50}$$

$$F_q(t) = K_0 x_0 \omega \left[c_3 e^{s_1 t} + c_4 e^{s_2 t}\right] \tag{51}$$

5 Comparison between the CFD model and the analytical model

In this section, a comparison between the analytical model and the CFD model is made to verify the analytical model. The CFD model is established by ADINA. ADINA is an advanced tool for the fluid-structure interaction problem. The fluid model and structure model should be established separately. A sinusoidal displacement excitation is applied to the structure model, in which the amplitude is 1 mm, the surface of the piston is defined as the fluid–structure interface, and the yellow part in Fig. 5 is the fluid–structure interface. During the computation, the two models exchange dates at each time step. To save computational time, a 1/4 model is used. After finishing the computation, forces of all the nodes on the fluid–structure interface should be extracted. These forces are called the pressure gradient force. Because the CFD model is a 1/4 model, the final pressure gradient force should be multiplied by 4. The parameters of the CFD model are shown in Table 1.

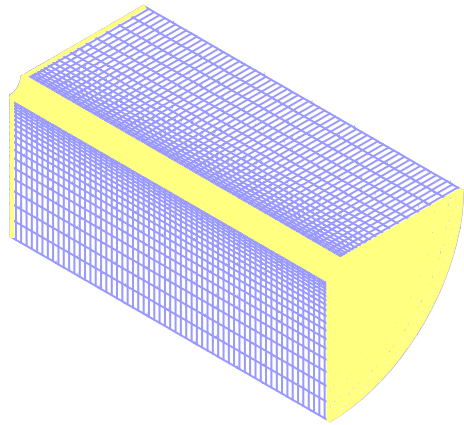

Fig. 5 Fluid–structure interface

Figure 6 shows a grid of the fluid in the damper. Figure 7 is the grid of the piston. To save computation time, a 1/4 CFD model is used. Figures 8, 9, 10 and 11 are the pressures in the damper of the four cases with viscosities of 1000, 900, 800, and 700 cst. Pressure in the left and right cavity is well distributed, while there is a pressure gradient in the orifice. The largest pressures in the damper are 1.61, 1.57, 1.50, and 1.42 MPa, respectively. The pressure in the damper decreases as the viscosity decreases because of the decreasing resistance. Figures 12, 13, 14 and 15 describe velocities in the damper. Velocity has the largest value in the orifice, but is equal to zero in the two cavities. The maximum velocities for the four cases are 27.06, 29.04, 31.10, and 33.37 m/s, respectively. Thus, the velocity decreases with decreasing viscosity. The reason is that when the viscosity increases, the fluidity of the silicone oil in the damper decreases. There is a diffusion region near the exit of the orifice due to the expansion of the cross section.

Table 1 Parameters of the CFD model

Case	Parameter	Value
1	d	2 mm
	Lg	30 mm
	ν	1000 cst
	x_0	1 mm
	f	50 Hz
2	d	2 mm
	Lg	30 mm
	ν	900 cst
	x_0	1 mm
	f	50 Hz
3	d	2 mm
	Lg	30 mm
	ν	800 cst
	x_0	1 mm
	f	50 Hz
4	d	2 mm
	Lg	30 mm
	ν	700 cst
	x_0	1 mm
	f	50 Hz

$D = 25$ mm, $L = 50$ mm, $\rho = 903\,\mathrm{Kg/m^3}$, $\beta = 100\,\mathrm{MPa}$

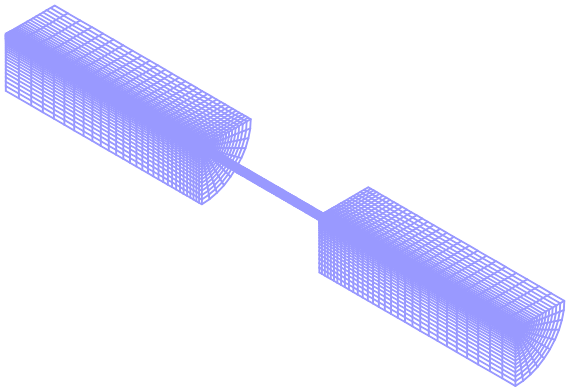

Fig. 6 Grid of the fluid in the damper

The length of the diffusion region increases as the viscosity increases. Pressure gradient forces of different viscosities are shown in Figs. 16, 17, 18 and 19. The pressure gradient force has the largest value of 1783 N when the viscosity is 1000 cst, it has the smallest value of 1721 N when the viscosity is 700 cst. It is shown that the pressure gradient force decays as the viscosity decreases. In the first vibration cycle (0–0.02 s), the

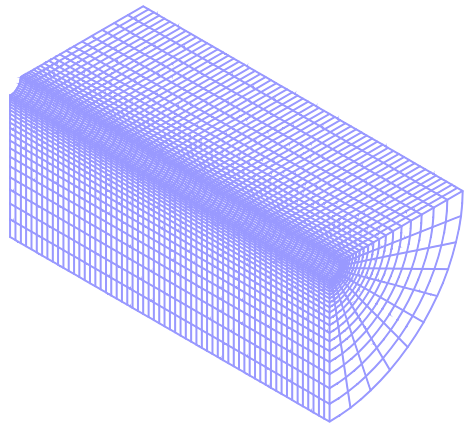

Fig. 7 Grid of the piston

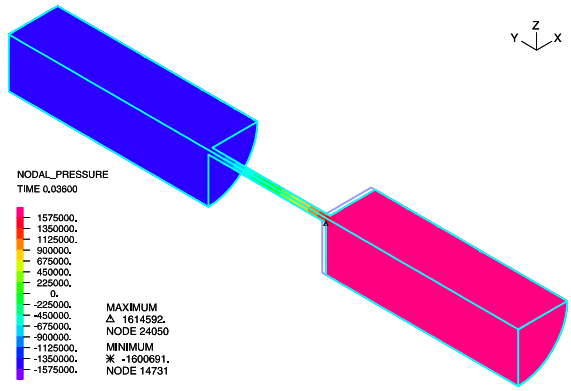

Fig. 8 Pressure in the damper (case 1)

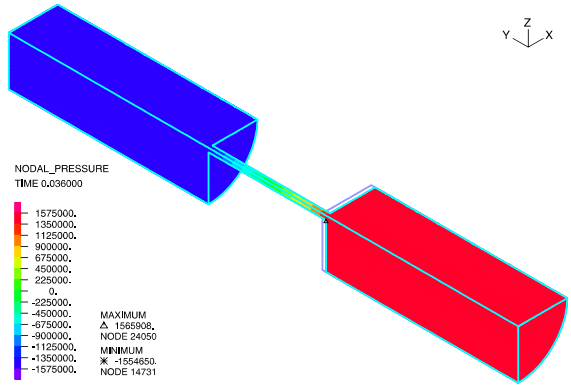

Fig. 9 Pressure in the damper (case 2)

amplitude of the pressure gradient force is small compared with the amplitude of the steady state because the direction of the transient force is opposite to that of the pressure gradient force. The transient force decays with time, which is consistent with the theory presented in Sect. 3.

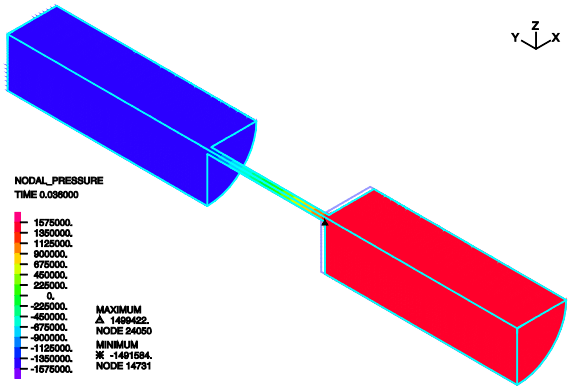

Fig. 10 Pressure in the damper (case 3)

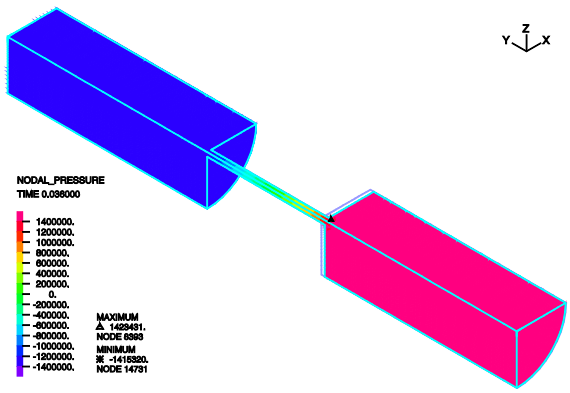

Fig. 11 Pressure in the damper (case 4)

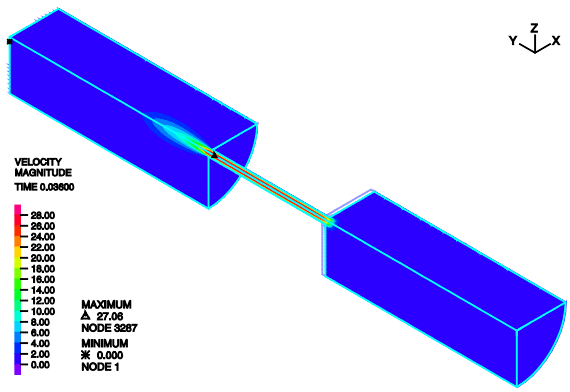

Fig. 12 Velocity in the damper (case 1)

Table 2 shows the relative errors of the pressure gradient force between the CFD model and the analytical model. The largest error is 5.05%. The smallest relative error is 2.96%. It is shown that the analytical model can describe the dynamic characteristics of single-tube micro-vibration isolators exactly.

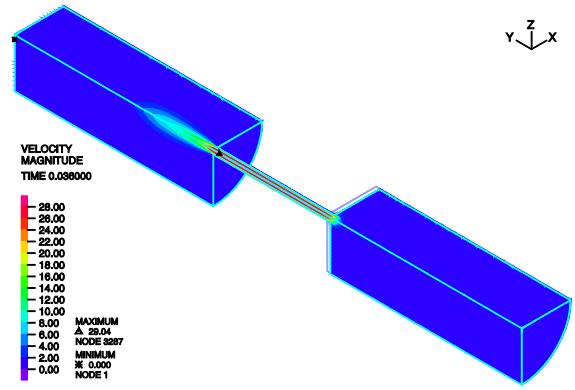

Fig. 13 Velocity in the damper (case 2)

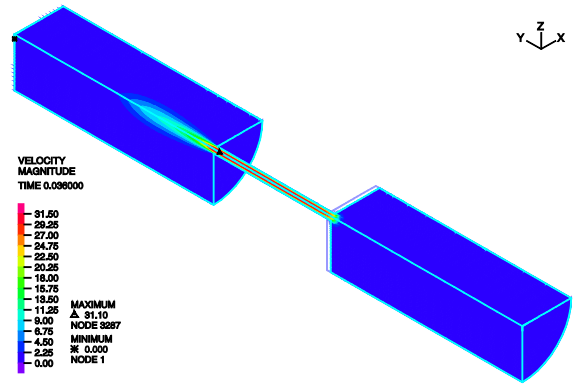

Fig. 14 Velocity in the damper (case 3)

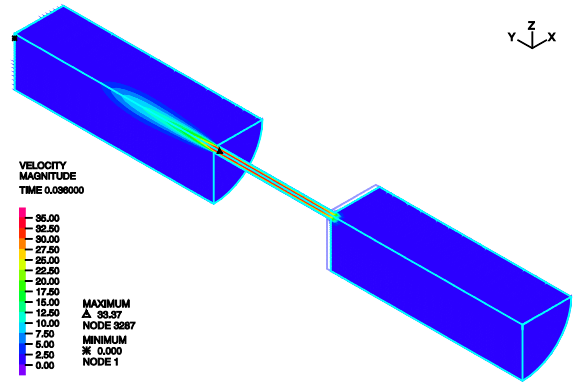

Fig. 15 Velocity in the damper (case 4)

In this section, the nonlinear damping force and nonlinear elastic force will be analyzed for different values of parameters.

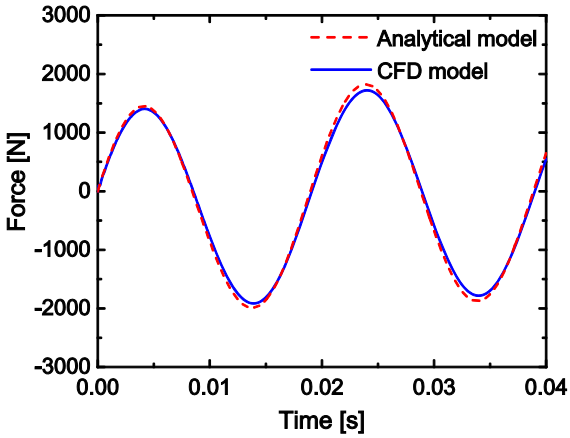

Fig. 16 Comparison of the pressure gradient force from the analytical model and the CFD model (case 1)

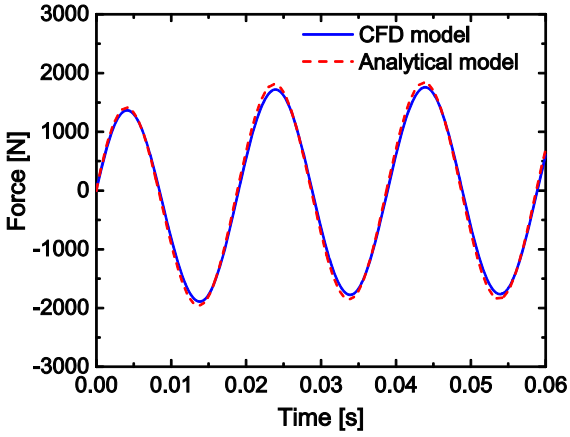

Fig. 17 Comparison of the pressure gradient force from the analytical model and the CFD model (case 2)

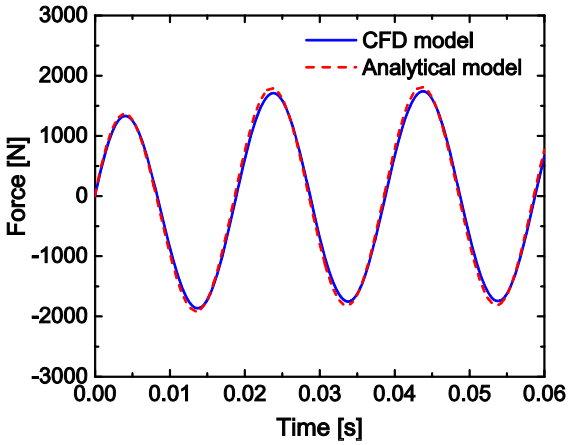

Fig. 18 Comparison of the pressure gradient force from the analytical model and the CFD model (case 3)

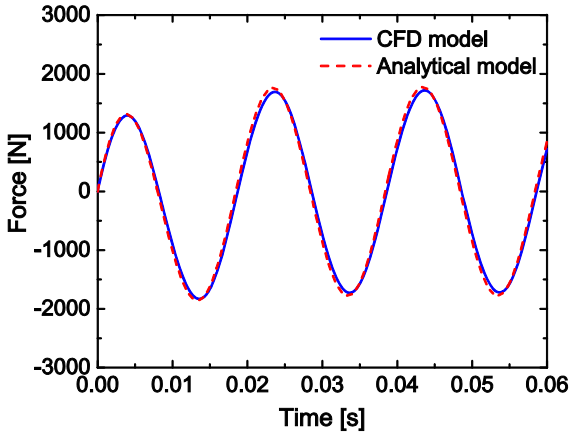

Fig. 19 Comparison of the pressure gradient force from the analytical model and the CFD model (case 4)

Table 2 Relative errors of the CFD model and analytical model

Viscosity	700 cst	800 cst	900 cst	1000 cst
Analytical model	1772 N	1812 N	1841 N	1873 N
CFD model	1721 N	1745 N	1764 N	1783 N
Relative error	2.96%	3.84%	4.37%	5.05%

6 Decomposition of the pressure gradient force

According to the derivation in Sect. 4, the pressure gradient force can be divided into an elastic force, a damping force, and a transient force. The elastic force provides stiffness, the damping force provides damping, and the transient force decays with time. Two cases are studied. The model parameters for these two cases are shown in Table 3. The difference between the two cases is the diameter of the orifice. The diameter of case 1 is 5 mm, and the diameter of case 2 is 2 mm, while the other parameters remain the same. In each case, we studied the pressure gradient force while considering and ignoring the entrance effect.

Figure 20 shows the pressure gradient force F_{pressure} when considering the entrance effect (case 1, diameter of the orifice is 5 mm). From 0 to 0.02 s, there is an oscillation phenomenon because the transient force oscillates significantly at the beginning. The pressure gradient force can be divided into a nonlinear damping force F_{damp}, a nonlinear elastic force F_{elastic}, and a transient force $F_{\text{transient}}$. It can be seen from Fig. 20 that the curve has some differences compared to the

Table 3 Model parameters

Case	Parameter	Value
1	d	5 mm
	Lg	10 mm
	ν	500 cst
	x_0	1 mm
	f	50 Hz
2	d	2 mm
	Lg	10 mm
	ν	500 cst
	x_0	1 mm
	f	50 Hz

$D = 25$ mm, $L = 50$ mm, $\rho = 903\,\mathrm{Kg/m^3}$, $\beta = 100$ MPa

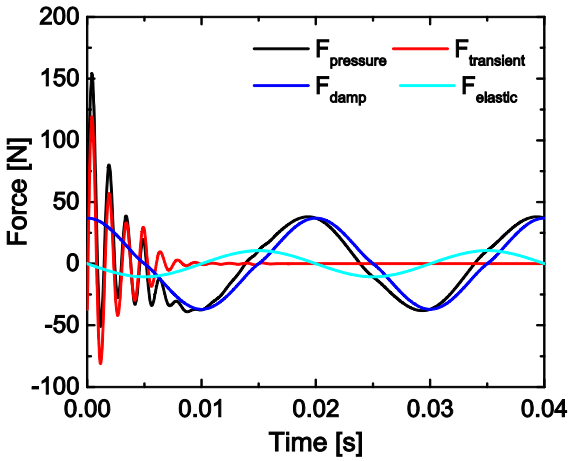

Fig. 20 Pressure gradient force considering the entrance effect (case 1)

sinusoidal curve due to the nonlinear damping force and the nonlinear elastic force. The reason is that when the entrance effect is considered, there is a nonlinear term in the resistance, and the pressure gradient force becomes a nonlinear force.

Figure 21 shows the pressure gradient force F_{pressure} without considering the entrance effect (case 1, diameter of the orifice is 5 mm). It can be seen from Fig. 21 that the pressure gradient force is sinusoidal. This means that the pressure gradient force is a linear force. The reason is that if the entrance effect is not considered, the damping force and elastic force have linear relationships with velocity and displacement. The pressure gradient force F_{pressure} can be divided into the linear damping force F_{damp}, the linear elastic force F_{elastic} and a transient force.

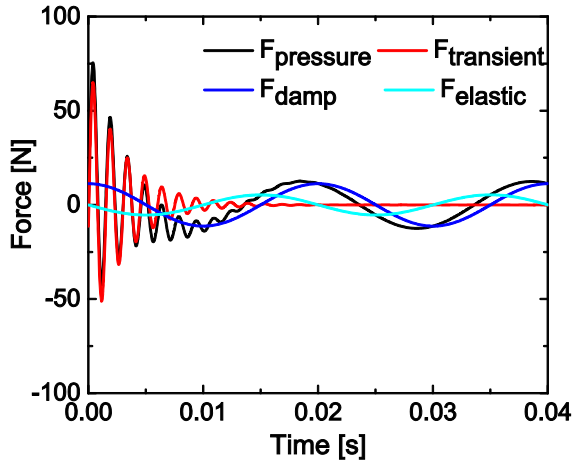

Fig. 21 Pressure gradient force without considering the entrance effect (case 1)

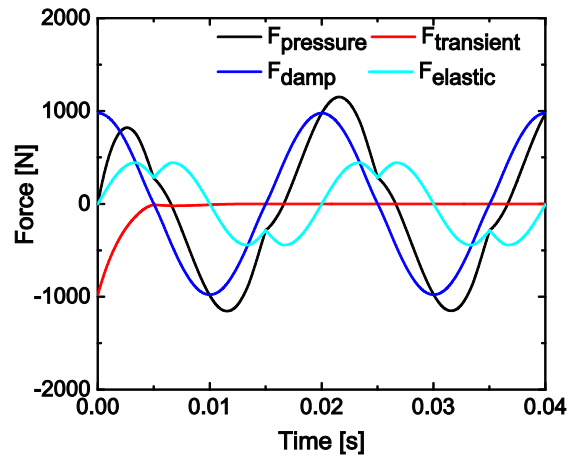

Fig. 22 Pressure gradient force considering the entrance effect (case 2)

Figure 22 shows the pressure gradient force considering the entrance effect (case 2, diameter of the orifice is 2 mm). The nonlinear elastic force is very clear, while the nonlinear damping force is not substantial. In this case, the transient force decays with time exponentially because when $\Delta > 0$, the characteristic roots are real roots and the transient force contains the exponential term. It can be seen from Fig. 22 that the pressure gradient force is a nonlinear force. This is more clear than in case 1 because when the diameter of the orifice decreases, the velocity in the orifice increases, so the nonlinear term in Eq. (25) also increases.

Figure 23 shows the pressure gradient force without considering the entrance effect (case 2, diameter of the

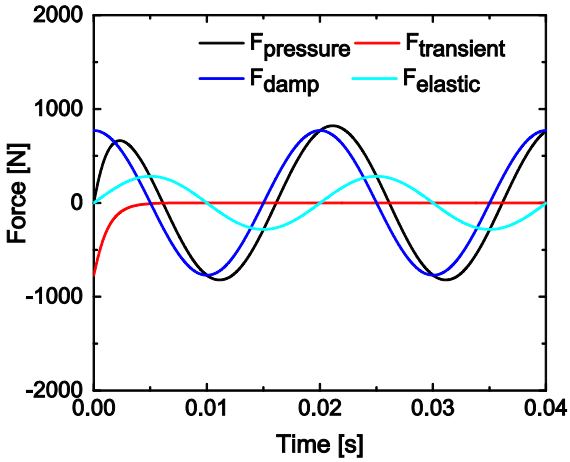

Fig. 23 Pressure gradient force without considering the entrance effect (case 2)

Table 4 Model parameters

Case	Parameter	Value
1	d	2 mm
	Lg	10 mm
	ν	200 cst
	x_0	1 mm
	f	1 Hz
2	d	2 mm
	Lg	10 mm
	ν	200 cst
	x_0	1 mm
	f	5 Hz
3	d	2 mm
	Lg	10 mm
	ν	200 cst
	x_0	1 mm
	f	50 Hz

$D = 25$ mm, $L = 50$ mm, $\rho = 903\,\mathrm{Kg/m^3}$, $\beta = 100$ MPa

orifice is 2 mm). It can be seen from the figure that the curve is a sinusoidal curve, which means that the pressure gradient force is a linear force. Because the entrance effect is not considered, the damping force and elastic force are linear forces too.

A comparison between the nonlinear pressure gradient force and the linear pressure gradient force is made at different frequencies. Model parameters are shown in Table 4. The frequency of case 1, 2, and 3 is 1, 5, 50 Hz, respectively.

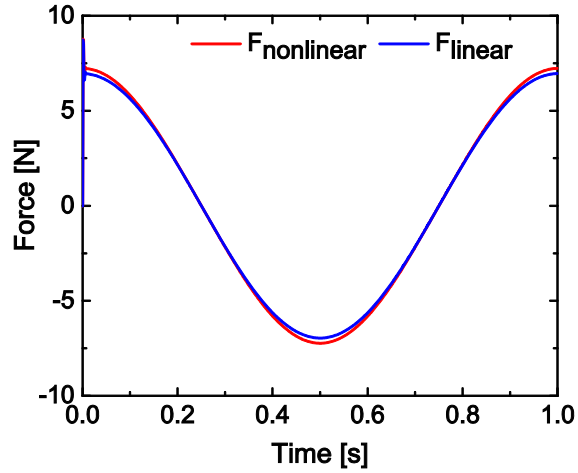

Fig. 24 Comparison between the linear and nonlinear pressure gradient forces (case 1)

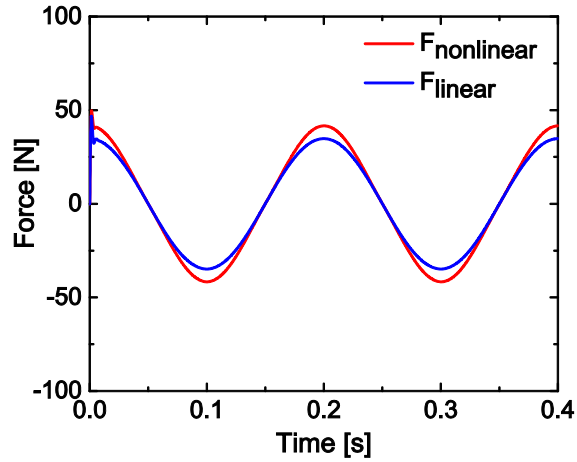

Fig. 25 Comparison between the linear and nonlinear pressure gradient forces (case 2)

Figure 24 is a comparison between the linear pressure gradient force and the nonlinear pressure gradient force, with a frequency of 1 Hz. There is an oscillation at the beginning due to the transient force, as seen in the figure. In addition, the linear pressure gradient force and the nonlinear pressure gradient force are nearly the same because when the frequency is low, the velocity in the orifice is low, the nonlinear term in Eq. (25) is small, and the resistances (both when the entrance effect is considered and when it is not) are nearly the same. The amplitude of the pressure gradient force is 7 N.

Figure 25 compares the linear pressure gradient force and the nonlinear pressure gradient force for a frequency of 5 Hz. There are some differences. The

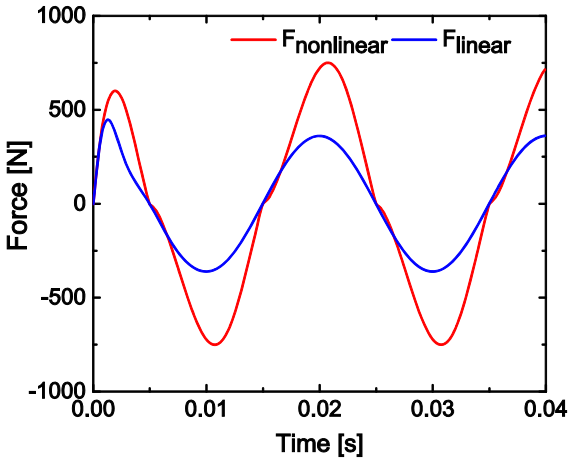

Fig. 26 Comparison between the linear and nonlinear pressure gradient forces (case 3)

amplitude of the nonlinear pressure gradient force is 42 N, while the amplitude of the linear pressure gradient force is 35 N. The figure shows that the nonlinear force is not substantial because the nonlinear term in the resistance is small for 5 Hz.

Figure 26 compares the linear pressure gradient force and the nonlinear pressure gradient force at a frequency of 50 Hz. The nonlinear force is substantial. The amplitude of the nonlinear pressure gradient force is 751 N, while the amplitude of the linear pressure gradient force is 361 N. The nonlinear pressure gradient force is twice the linear pressure gradient force. Therefore, there will be a large difference between the two models (both with and without considering the entrance effect). The reason is that when the viscosity is low at a high frequency, the entrance effect is substantial; therefore, it is necessary to consider the entrance effect in this scenario.

7 Hysteresis loop of pressure gradient force

A hysteresis loop can describe damping and stiffness intuitively. The area of a hysteresis loop represents the energy loss. The slope of the hysteresis represents the stiffness. In this section, a hysteresis loop of the pressure gradient force will be analyzed. The model that considers the entrance effect is used. The model parameters are shown in Table 5. Five cases are analyzed. Case 1 is an analysis of hysteresis loops for different diameters. Case 2 is an analysis of hysteresis loops for different lengths. Case 3 is an analysis of hysteresis loops for different viscosities. Case 4 is an analysis of hysteresis loops for different amplitudes. Case 5 is an analysis of hysteresis loops for different frequencies.

Table 5 Model parameters

Case	Parameter	Value
1	d	1.0/1.2/1.4/1.6 mm
	Lg	10 mm
	ν	200 cst
	x_0	1 mm
	f	50 Hz
2	d	2 mm
	Lg	5/10/15/20 mm
	ν	200 cst
	x_0	1 mm
	f	50 Hz
3	d	2 mm
	Lg	10 mm
	ν	100/200/300/400 cst
	x_0	1 mm
	f	50 Hz
4	d	2 mm
	Lg	10 mm
	ν	200 cst
	x_0	0.6/0.8/1.0/1.2 mm
	f	50 Hz
5	d	2 mm
	Lg	10 mm
	ν	200 cst
	x_0	1 mm
	f	10/20/30/40 Hz

$D = 25$ mm, L =50mm, $\rho = 903\text{Kg/m}^3$, $\beta = 100$MPa

Figure 27 shows hysteresis loops for different diameters. The diameters are 1.0, 1.2, 1.4, and 1.6 mm. The frequency is 50 Hz. The area of the hysteresis loop increases as the diameter increases, which means that more vibrational energy will be consumed, but the slope of the hysteresis loop decreases, the reason is that when the diameter increases, more silicone oil flows through the orifice, while at the same time, less silicone oil will be compressed. Figure 28 shows hysteresis loops for different lengths. The lengths are 5, 10, and 20 mm. The frequency is 50 Hz. The area of the hysteresis loop increases as the length of orifice increases. This means that more vibrational energy will be consumed as the length increases. The hysteresis loop is not elliptical

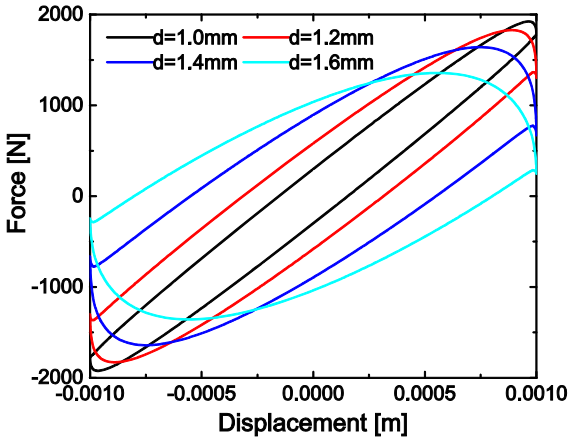

Fig. 27 Hysteresis loops for different diameters (case 1)

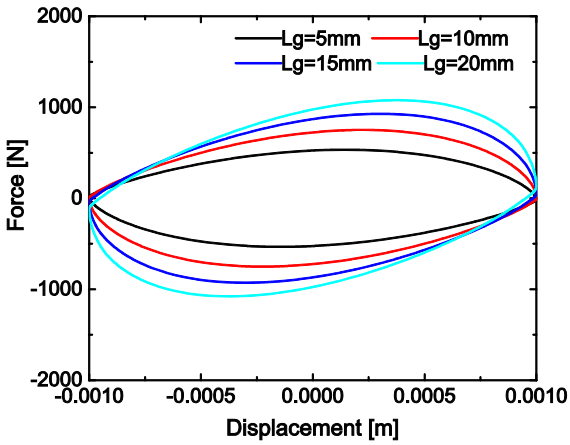

Fig. 28 Hysteresis loops for different lengths (case 2)

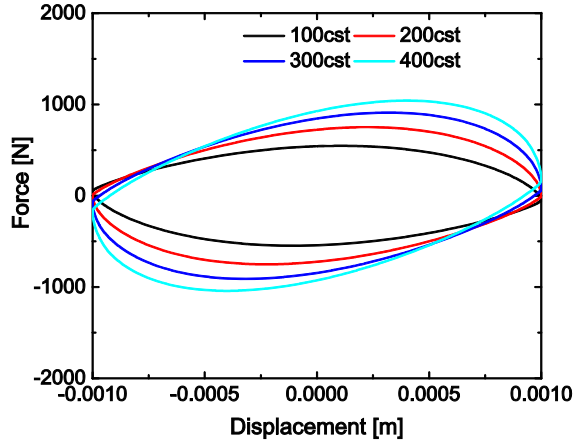

Fig. 29 Hysteresis loops for different viscosities (case 3)

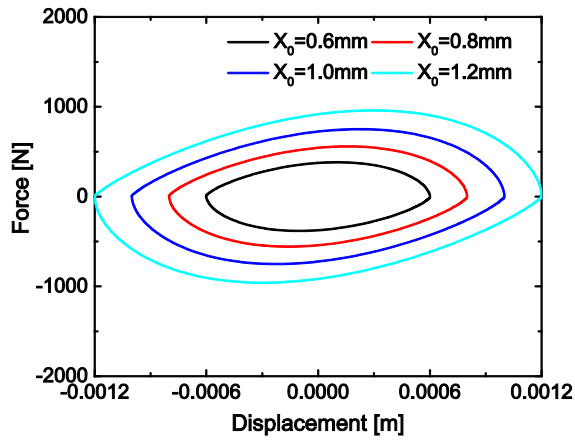

Fig. 30 Hysteresis loop of different amplitudes (case 4)

because of the nonlinear pressure gradient force. Furthermore, the slope of the hysteresis loop increases as the length increases, which means that the stiffness will increase because the resistance increases as the length increases and more silicone oil will be compressed.

Figure 29 shows hysteresis loops for different viscosities. The viscosities are 100, 200, 300, and 400 cst. The frequency is 50 Hz. The area of the hysteresis loop increases as the viscosity increases. It means that more vibrational energy will be consumed when the viscosity increases. The slope of the hysteresis loop increases as the length increases, which means that the stiffness increases as the viscosity increases. The resistance increases as the viscosity increases, and more silicone oil will be compressed.

Figure 30 shows hysteresis loops for different amplitudes. The amplitudes are 0.6, 0.8, 1.0, and 1.2 mm. These curves are concentric. This reveals that the stiffness is constant at different amplitudes when the frequency is constant. The area of the hysteresis loop increases as the amplitude increases, which means that more vibrational energy will be consumed.

Figure 31 shows hysteresis loops for different frequencies. The frequencies are 10, 20, 30, and 40 Hz. It can be seen from the figure that the hysteresis loop is not elliptical due to the nonlinear pressure gradient force. The area of the hysteresis loop increases as the frequency increases, which means that more vibrational energy will be consumed. When the frequency increases, the velocity in the orifice increases, and the damping force also increases. In addition, the slope of the hysteresis loop is not significant because when the frequency is low, little silicone oil will be compressed.

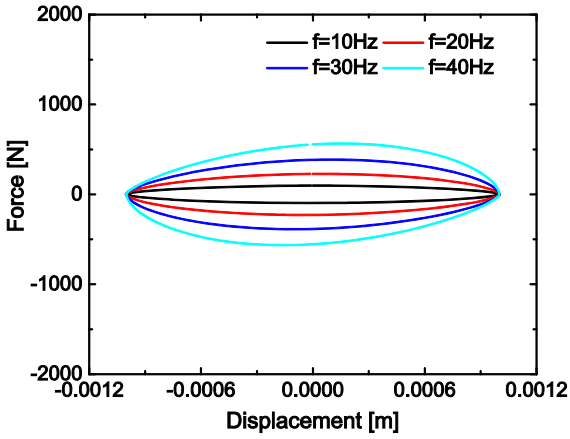

Fig. 31 Hysteresis loops for different frequencies (case 5)

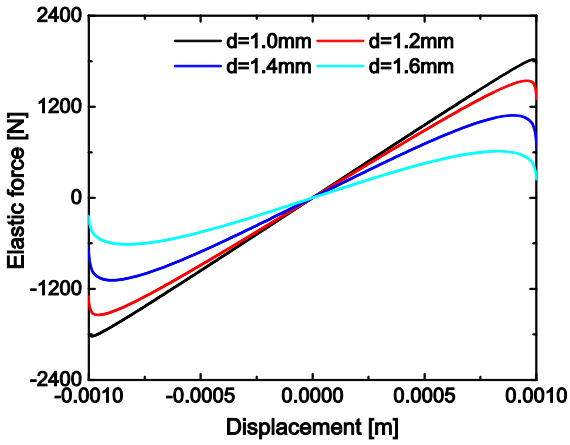

Fig. 32 Nonlinear elastic forces for different diameters (case 1)

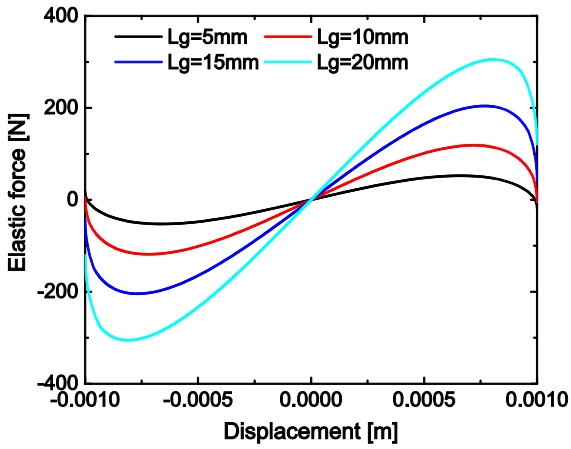

Fig. 33 Nonlinear elastic forces for different lengths (case 2)

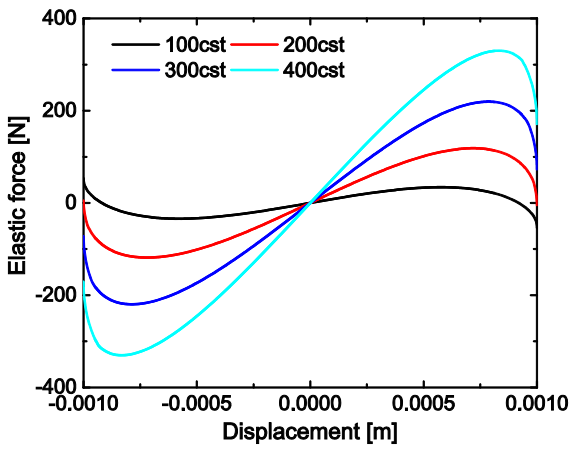

Fig. 34 Nonlinear elastic forces for different viscosities (case 3)

8 Nonlinear elastic force

According to the derivation in Sect. 2, when considering the entrance effect, the pressure gradient force is nonlinear. In this section, the nonlinear elastic forces for the 5 cases that are shown in Table 5 will be analyzed. The model parameters are shown in Table 5. Figure 32 shows the nonlinear elastic force for different diameters. The diameters are 1.0, 1.2, 1.4, and 1.6 mm. It can be seen from the figure that the nonlinear elastic force decreases as the diameter increases for the same frequency because when the diameter increases, the amount of silicone oil that is compressed decreases and more silicone will pass through the orifice.

Figure 33 shows the nonlinear elastic forces for different lengths. The lengths are 5, 10, 15, and 20 mm. It can be seen from the figure that the nonlinear elastic force increases as the length increases at the same frequency. The reason is that when the length increases, the resistance increases and more silicone oil will be compressed.

Figure 34 shows the nonlinear elastic forces for viscosities of 100, 200, 300, and 400 cst. The nonlinear elastic force increases as the viscosity increases at the same frequency because when the viscosity increases, the resistance increases and more silicone oil will be compressed.

Figure 35 shows the nonlinear elastic forces of different amplitudes, 0.6, 0.8, 1.0, and 1.2 mm. It can be seen from the figure that the nonlinear elastic force increases as the amplitude increases for the same frequency, because when the amplitude increases, the

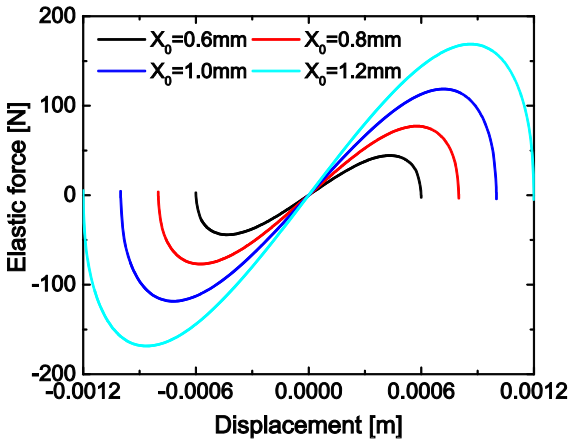

Fig. 35 Nonlinear elastic forces for different amplitudes (case 4)

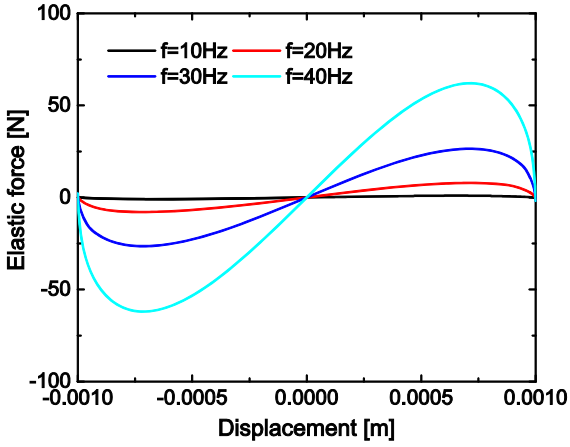

Fig. 36 Nonlinear elastic forces for different frequencies (case 5)

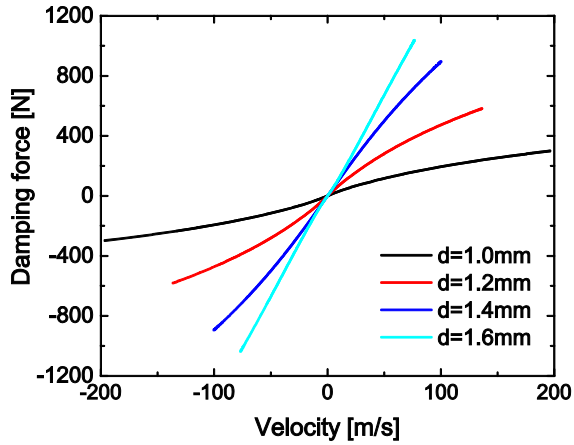

Fig. 37 Nonlinear damping force for different diameters (case 1)

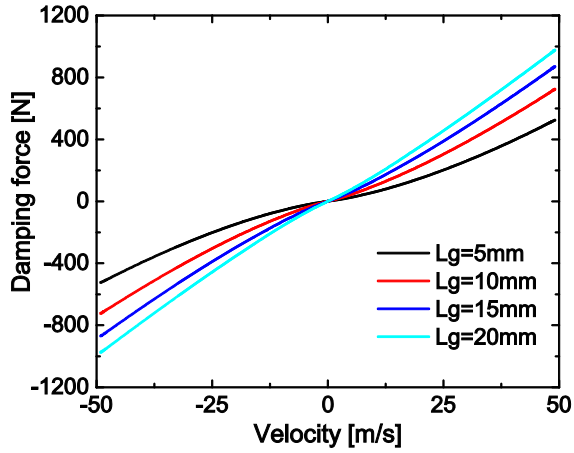

Fig. 38 Nonlinear damping force for different lengths (case 2)

velocity increases, leading to increased resistance and more compression of the silicone oil.

Figure 36 shows the nonlinear elastic forces for different frequencies. The elastic force significantly increases as the frequency increases. The reason is when the frequency increases, the velocity also increases, leading to an increased resistance; therefore, more silicone oil will be compressed. However, when the frequency increases to a certain value, the stiffness does not increase.

9 Nonlinear damping force

According to the derivation in Sect. 4, the damping force is a function of the velocity. In this section, nonlinear elastic forces for the 5 cases shown in Table 5 will be analyzed. The model parameters are shown in Table 5.

Figure 37 shows nonlinear damping forces for different diameters of 1.0, 1.2, 1.4, and 1.6 mm. The damping force increases as the diameter increases. However, this trend is opposite to that of the elastic force. The reason is that when the diameter increases, the resistance decreases because the silicone oil flows better through the orifice.

Figure 38 shows the nonlinear damping force for different lengths. The damping force increases as the length increases. When the length is short, the nonlinear damping force is substantial; however, when the length is long, the nonlinear damping force is not substantial. The reason is when the length increases, the

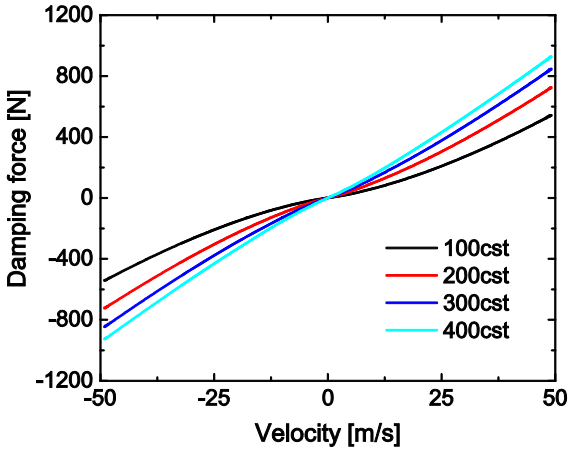

Fig. 39 Nonlinear damping force for different viscosities (case 3)

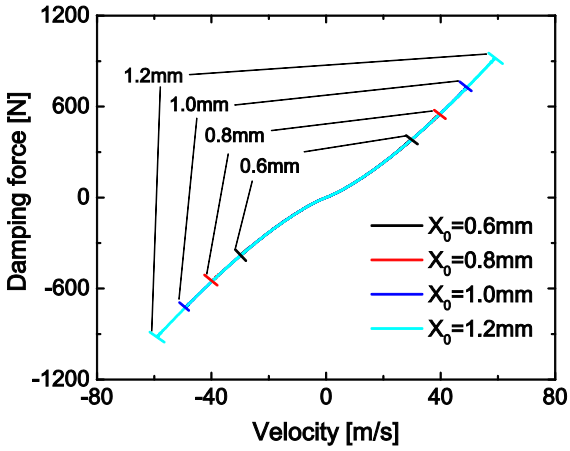

Fig. 40 Nonlinear damping force for different amplitudes (case 4)

resistance increases, velocity in the orifice decreases, and the nonlinear term in the resistance decreases.

Figure 39 shows the nonlinear damping force for different viscosities. The damping force increases as the viscosity increases. It is clear when the viscosity is small; however, the nonlinear force is not substantial when the viscosity increases because when the viscosity increases, the velocity in the orifice decreases, and the nonlinear term in the resistance also decreases.

Figure 40 shows the damping force for different amplitudes. When the amplitude increases, the shape of the curve does not change, but the amplitude of the nonlinear damping force increases. This occurs because as the amplitude increases, the nonlinear damping coefficient does not change, but the velocity increases, which

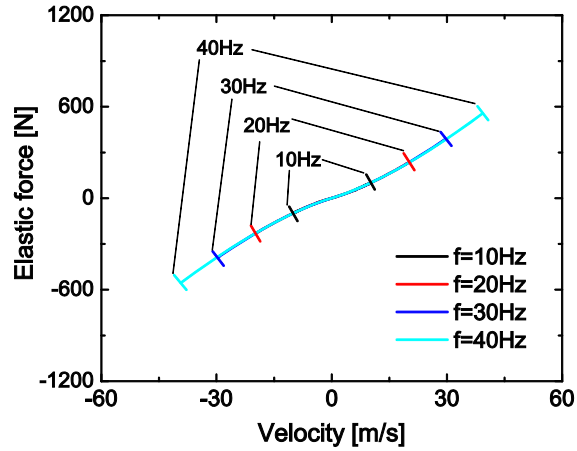

Fig. 41 Nonlinear damping force for different frequencies (case 5)

leads to an increase in the amplitude of the nonlinear damping force.

Figure 41 shows the damping force for different frequencies. It can be seen from the figure that the curves of the four frequencies nearly coincide with each other, but if the frequency continues to increase, the difference will become substantial. This occurs because when the frequency is low, the damping coefficient changes slowly. When viscosity is 200 cst, the nonlinear damping force will change slowly, but when the frequency continues to increase, the damping coefficient changes quickly, so the difference is very substantial.

10 Conclusions

In this paper, a nonlinear dynamic model of a micro-vibration fluid viscous damper has been proposed. While considering the entrance effect in the damping orifice, the nonlinear damping force and the nonlinear elastic force are analyzed. The results reveal the following:

(1) The pressure gradient force contains a damping force, an elastic force, and a transient force. The elastic force provides stiffness, the damping force consumes vibration energy, and the transient force decays with time. The transient force decays with time according to an exponential law or oscillation law. It depends on the diameter and length of the damping orifice and the viscosity of the silicone oil.

(2) When ignoring the entrance effect in the orifice, the damping force and elastic force are linear forces. When considering the entrance effect in the damping orifice, the damping force and elastic force are nonlinear forces. At low frequencies, the pressure gradient forces in the two cases are nearly the same, but at high frequencies, they are quite different.
(3) The nonlinear damping force and the nonlinear elastic force have a relationship with the diameter and length of the damping orifice, viscosity, amplitude, and frequency. The nonlinear damping force and elastic force change with these parameters.

The results sufficiently demonstrate the nonlinear dynamic characteristics of a single-tube fluid viscous damper. The model that considers the entrance effect can be used to design the nonlinear damping and stiffness of micro-vibration fluid viscous dampers. In addition, the bulk modulus of the fluid is also considered in this model; therefore, the model can be used in low-frequency and high-frequency applications.

Acknowledgements The authors gratefully acknowledge the support of National Basic Research Program of China (No. 2013CB733004) and National Defense Basic Research Plan of China (No. A0320110016).

References

1. Kamesh, D., Pandiyan, R., Ghosal, A.: Modeling, design and analysis of low frequency platform for attenuating micro vibration in spacecraft. J. Sound Vib. **329**(17), 3431–3450 (2010)
2. Davis, P., Cunningham, D., Harrell, J.: Advanced 1.5 Hz passive viscous isolation system. In: 35th Structures, Structural Dynamics, and Materials Conference, vol. 32, No. 5Suppl, pp. 2655–2665 (2013)
3. Davis, L.P., Carter, D.R., Hyde, T.T.: Second-generation hybrid D-strut. In: Proceedings of SPIE, pp. 161–175 (1995)
4. Stabile, A., Aglietti, G.S., Richardson, G.: Electromagnetic damper design using a multiphysics approach. Proc. SPIE. **9431**(20), 1–9 (2015)
5. Stabile, A., Aglietti, G.S., Richardson, G., Smet, G.: Design and verification of a negative resistance electromagnetic shunt damper for spacecraft micro vibration. J. Sound Vib. **386**, 38–49 (2017)
6. Stabile, A., Aglietti, G.S., Richardson, G., Smet, G.: A 2-collinear-DoF strut with embedded negative-resistance electromagnetic shunt dampers for spacecraft micro vibration. Smart Mater. Struct. **26**(4), 045031 (2017)
7. Lee, D.-O., Park, G., Han, J.-H.: Experimental study on on-orbit and launch environment vibration isolation performance of a vibration isolator using bellows and viscous fluid. Aerosp. Sci. Technol. **45**, 1–9 (2015)
8. Lee, D.-O., Park, G., Han, J.-H.: Hybrid isolation of micro vibrations induced by reaction wheels. J. Sound Vib. **363**, 1–17 (2016)
9. Wang, J., Zhao, S., Wu, D.: Performance of a type of nonlinear fluid micro vibration isolators. J. Aerosp. Eng. **28**(6), 04015002 (2015)
10. Shi, W.-K., Qian, C., Chen, Z.-Y., Cao, Y., Zhang, H.: Modeling and dynamic properties of a four-parameter Zener model vibration isolator. Shock Vib. **2016**, 1–16 (2016)
11. Narkhede, D.I., Sinha, R.: Behavior of nonlinear fluid viscous dampers for control of shock vibrations. J. Sound Vib. **333**(1), 80–98 (2014)
12. Hou, C.-Y.: Behavior explanation and a new model for nonlinear viscous fluid dampers with a simple annular orifice. Arch. Appl. Mech. **82**(1), 1–12 (2011)
13. Peng, Z.K., Lang, Z.Q., Zhao, L., Billings, S.A., Tomlinson, G.R., Guo, P.F.: The force transmissibility of MDOF structures with a non-linear viscous damping device. Int. J. Nonlinear Mech. **46**(10), 1305–1314 (2011)
14. Wolfe, R.W., Yun, H.B., Masri, S., Tasbihgoo, F., Benzoni, G.: Fidelity of reduced-order models for large-scale nonlinear orifice viscous dampers. Struct. Control Health Monit. **15**(8), 1143–1163 (2008)
15. Farjoud, A., Ahmadian, M., Craft, M., Burke, W.: Nonlinear modeling and experimental characterization of hydraulic dampers: effects of shim stack and orifice parameters on damper performance. Nonlinear Dyn. **67**(2), 1437–1456 (2011)
16. Hou, C.-Y.: Fluid dynamics and behavior of nonlinear viscous fluid dampers. J. Struct. Eng. **134**(1), 56–63 (2008)
17. Narkhede, D.I., Sinha, R.: Influence of shock impulse characteristics on vibration control using nonlinear fluid viscous dampers. J. Vib. Control **23**(9), 1463–1479 (2015)
18. Shum, K.M.: Tuned vibration absorbers with nonlinear viscous damping for damped structures under random load. J. Sound Vib. **346**, 70–80 (2015)
19. Guo, P.F., Lang, Z.Q., Peng, Z.K.: Analysis and design of the force and displacement transmissibility of nonlinear viscous damper based vibration isolation systems. Nonlinear Dyn. **67**(4), 2671–2687 (2012)
20. Lang, Z.Q., Jing, X.J., Billings, S.A., Tomlinson, G.R., Peng, Z.K.: Theoretical study of the effects of nonlinear viscous damping on vibration isolation of sdof systems. J. Sound Vib. **323**(1–2), 352–365 (2009)
21. Lv, Q., Yao, Z.: Analysis of the effects of nonlinear viscous damping on vibration isolator. Nonlinear Dyn. **79**(4), 2325–2332 (2014)
22. Goldasz, J., Alexandridis, A.A.: Medium- and high-frequency analysis of magnetorheological fluid dampers. J. Vib. Control **18**(14), 2140–2148 (2011)